3-7-2022

Location of cobalt impurities in the surface oxide of stainless steel 316L and metal release in synthetic biological fluids

Xuying Wang

Jonas Hedberg

Heng-Yong Nie

Mark C. Biesinger

Inger Odnevall

See next page for additional authors

Authors

Xuying Wang, Jonas Hedberg, Heng-Yong Nie, Mark C. Biesinger, Inger Odnevall, and Yolanda S. Hedberg

Materials & Design 215 (2022) 110524

Contents lists available at ScienceDirect

Materials & Design

journal homepage: www.elsevier.com/locate/matdes

Location of cobalt impurities in the surface oxide of stainless steel 316L and metal release in synthetic biological fluids

Xuying Wang [a], Jonas Hedberg [b], Heng-Yong Nie [b,c], Mark C. Biesinger [b,d], Inger Odnevall [a,e,f,*], Yolanda S. Hedberg [a,b,d,*]

[a] KTH Royal Institute of Technology, School of Engineering Sciences in Chemistry, Biotechnology and Health, Department of Chemistry, Division of Surface and Corrosion Science, Drottning Kristinas v. 51, SE-10044 Stockholm, Sweden
[b] Surface Science Western, The University of Western Ontario, 999 Collip Circle, London, Ontario N6G 0J3, Canada
[c] Dept. of Physics and Astronomy, The University of Western Ontario, 1151 Richmond Str, London, Ontario N6A 5B7, Canada
[d] Dept. of Chemistry, The University of Western Ontario, 1151 Richmond Str, London, Ontario N6A 5B7, Canada
[e] AIMES - Center for the Advancement of Integrated Medical and Engineering Sciences at Karolinska Institutet and KTH Royal Institute of Technology, Stockholm, Sweden
[f] Department of Neuroscience, Karolinska Institutet, SE-171 77 Stockholm, Sweden

HIGHLIGHTS

- Bioaccessibility of cobalt in stainless steels important from a legislative view.
- Surface oxide and metal release of austenitic stainless steel 316L studied.
- Metallic cobalt homogeneously co-located with nickel beneath the surface oxide.
- Cobalt traces released with other metals upon surface reformation and passivation.
- Surface enrichment of cobalt due to precipitation of released cobalt in PBS.

GRAPHICAL ABSTRACT

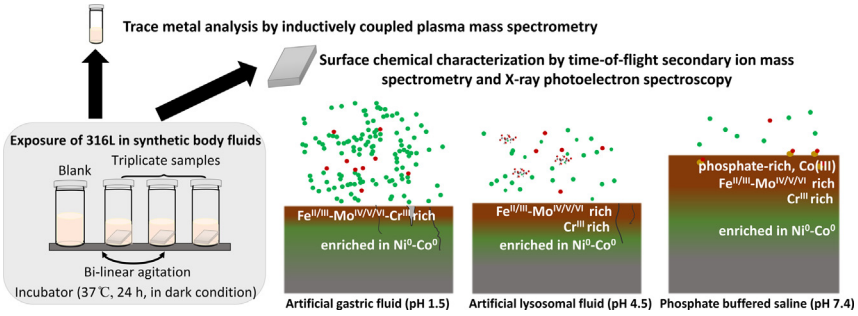

ARTICLE INFO

Article history:
Received 1 November 2021
Revised 8 February 2022
Accepted 3 March 2022
Available online 7 March 2022

Keywords:
Stainless steel
Cobalt
ToF-SIMS
XPS

ABSTRACT

Since 2021, cobalt (Co) is in Europe classified as carcinogen in quantities exceeding 0.1 wt-%. This affects nickel-rich stainless steels, which contain about 0.2 wt-% Co impurities. Previous findings show the bioaccessibility of Co in stainless steel to be primarily determined by the corrosion resistance. It has been unclear whether Co is distributed heterogeneously in the alloy and the outermost surface and whether a specific location would pose a risk for Co release under specific exposure conditions. This study aimed at locating Co in stainless steel 316L (0.2 wt-% Co) surfaces prior to and after exposure to different synthetic body fluids for 24 h at 37 °C. Time-of-flight secondary ion mass spectrometry (ToF-SIMS), X-ray photoelectron spectroscopy (XPS), and inductively coupled plasma mass spectrometry (ICPMS) investigated the location of Co in the surface oxide and extent of release along with other metals (iron, chromium, nickel, and manganese) into synthetic biological fluids (gastric fluid, pH 1.5; lysosomal fluid,

Abbreviations: ALF, Artificial Lysosomal Fluid; BE, Binding Energy; Co, Cobalt; Fe, Iron; GST, Artificial Gastric Fluid; ICPMS, Inductively Coupled Plasma Mass Spectrometry; IMFP, Inelastic Mean Free Path; LOD, Limit of Detection; LOQ, Limit of Quantification; Mn, Manganese; Mo, Molybdenum; Ni, Nickel; PBS, Phosphate Buffered Saline; REACH, Registration, Evaluation, Authorisation and Restriction of Chemicals; ToF-SIMS, Time of Flight Secondary Ion Mass Spectrometry; XPS, X-ray Photoelectron Spectroscopy.

* Corresponding authors at: KTH Royal Institute of Technology, School of Engineering Sciences in Chemistry, Biotechnology and Health, Department of Chemistry, Division of Surface and Corrosion Science, Drottning Kristinas v. 51, SE-10044 Stockholm, Sweden (I. Odnevall) The University of Western Ontario, Department of Chemistry, 1151 Richmond Str, London, Ontario N6A 5B7, Canada (Y. Hedberg).

E-mail addresses: ingero@kth.se (I. Odnevall), yhedberg@uwo.ca (Y.S. Hedberg).

https://doi.org/10.1016/j.matdes.2022.110524

Passive films
Bioaccessibility

pH 4.5; phosphate buffered saline-PBS, pH 7.4). Co was homogeneously distributed along with metallic nickel beneath the surface oxide and co-released with other metals upon surface reformation and passivation. Exposure in PBS resulted in the incorporation of both Co and phosphate in the oxide.

1. Introduction

Stainless steels are iron (Fe) based alloys that exhibit a high corrosion resistance in various harsh environments and are used in a broad range of applications such as in food processing and in the human body [1–3]. The main alloying elements (e.g., chromium - Cr, nickel - Ni, manganese - Mn, molybdenum - Mo) govern the mechanical and corrosion properties. The ASTM 300-series contain Ni (6–20 wt%) to stabilize the austenitic (face centered cubic) crystal structure. Since cobalt (Co) is an unintentional impurity when mining Ni, Ni-rich stainless steel grades inevitably contain small amounts of Co (<0.3 wt%) [4,5]. Co usually remains in the melt during the smelting process and can therefore not be removed in an economically viable way. Except for applications in the nuclear industry [4], Co impurities have not shown any influence either on the function or corrosion resistance of stainless steels. They have therefore, to our best knowledge, not previously been investigated with regards to location and surface speciation of Co.

Under "Registration, Evaluation, Authorisation and Restriction of Chemicals" (REACH) [6], the chemical regulation of the European Union (EU), metals are described as substances for which registration is required to ensure safety from a health and environmental perspective. Registration dossiers under REACH include information on toxicological hazards, which are intimately connected to metal bioaccessibility. In this context, bioaccessibility means the amount of metal species that can be released under simulated physiological conditions and potentially be available for absorption into systemic circulation [7]. Since metal alloys such as stainless steel from a legislative perspective are considered as mixtures of metals, registration dossiers are not required. According to the Classification, Labelling and Packaging Regulation, Co is classified as a skin allergen (Skin Sens. 1), suspected of causing cancer (Carc. 1B), mutagenic (Muta. 2), toxic to reproduction (Repr. 1B), a respiratory sensitizer (Resp. Sens. 1), and suspected of causing long-lasting harmful effects to aquatic life (Aquatic Chronic 4) [8]. Alloys which contain more than 0.1 wt% Co (generic concentration limit) are since Oct 1, 2021, classified as Carc. 1B [8,9]. A content of at least 0.1 wt% Co applies to many stainless steel grades, in particular Ni-containing stainless steels like the 300-series containing Co impurities. Discussions are under way to lower the generic concentration limit further to a specific concentration limit of 0.01 wt% Co. This would also affect other stainless steels and steel grades.

Triggered by the new regulation and the limited knowledge, studies on Co release (bioaccessibility), from a number of stainless steel grades were recently conducted in simulated body fluids of pH values ranging from 1.5 to 7.4, simulating different exposure scenarios including ingestion, inhalation, and skin contact [5,10]. Released amounts of Co from stainless steel 316L into an acidic medium simulating ingestion (pH 1.5) were 600-fold lower than expected based on its bulk content of Co [5]. While the trend in Co release among different steel grades generally inversely correlated with the corrosion resistance, no correlation was observed between the pitting corrosion resistance and the extent of Co release into synthetic body fluids (no applied potential) [5].

Metal release (as ions, complexes, and/or particles) is governed by different processes taking place at/within the surface oxide or at the metal interface including localized or uniform corrosion phenomena (metal oxidation), ligand-induced dissolution and/or physical processes such as wear, or their combinations [2]. As previously reported for native oxides on stainless steel [3,11,12], these oxides have a duplex character with an outer layer rich in Fe/Mo oxides and an inner layer enriched in Cr oxides with metallic Ni enriched at the metal/oxide interface [3,11–16]. The native oxide composition and thickness typically change with time upon immersion in an aqueous solution. The extent of Co impurities in stainless steels is very low and has previously not been studied to the same extent as other impurities such as carbon (forming Cr-rich carbides responsible for intergranular corrosion [17,18]) and sulfur (forming MnS inclusions important to pitting corrosion [19,20]). It is not known whether Co is enriched beneath the surface oxide in a similar way as Ni (non-oxidized) [3,11,13–15], enriched at grain boundaries (as precipitates), and/or homogenously or heterogeneously dispersed in the alloy and/or within the surface oxide. Its location will influence its ability to be released in a given medium.

The aim of this paper is to gain insight in the Co release process from stainless steel 316L by determining the location of Co impurities in the surface of stainless steel 316L upon exposure to three synthetic biological fluids of varying pH (artificial gastric fluid – GST [pH 1.5], artificial lysosomal fluid – ALF [pH 4.5], phosphate buffered saline – PBS [pH 7.4]). This was accomplished by using three complementary techniques, including time-of-flight secondary ion mass spectrometry (ToF-SIMS), X-ray photoelectron spectroscopy (XPS), and inductively coupled plasma mass spectrometry (ICPMS), to locate Co and characterize changes in composition and thickness of the surface oxide in relation to released concentrations of Co and other metals in the different fluids.

2. Materials and methods

2.1. Surface preparation and exposure in synthetic biological fluids

Cold-rolled stainless steel, grade ASTM 316L (EN 1.4404) with a composition (wt.-%) of 0.2% Co, 0.019% C, 0.9% Mn, 10% Ni, 17% Cr, 2% Mo, <0.00005% S, and balanced Fe (based on supplier information) was kindly provided by Outokumpu Stainless AB, Sweden. The material was cut into 2 mm thick 1.5 × 1.5 cm^2 coupons.

The coupons were grinded in sequence using SiC paper (200, 400, 800, 1600, and 4000 grit) followed by diamond polishing (6 μm and 3 μm). The coupons were then ultrasonically cleaned in acetone followed by ethanol for 5 min each, dried with nitrogen gas at room temperature, and aged in a desiccator (<10% relative humidity) for 24 h to ensure a reproducible air-formed surface oxide. Triplicate coupons and one blank sample (without any coupon) were exposed in parallel at 37 °C for each fluid in individual closed vessels for 24 h in an incubator (bi-linear shaking, 12° inclination, 22 cycles/min). The exposed surface area to solution volume ratio was in all cases 1 cm^2/mL, as stipulated in the EN 1811 standard of the European Nickel Directive [22] for Ni release testing to simulate skin contact [21]. Comparative surface analytical investigations were conducted on non-exposed coupons of the same surface preparation.

Studies were conducted in three different synthetic body fluids of different pH and expected influence on corrosion, including arti-

ficial gastric fluid (GST), artificial lysosomal fluid (ALF) and phosphate buffered saline (PBS). GST (pH 1.5) mimics the harsh conditions in the stomach [23]. ALF (pH 4.5) mimics intracellular conditions in the lung in conjunction with phagocytosis [24] and is hence relevant for the inhalation scenario and exposure to particles, e.g., wear debris. PBS (pH 7.4) mimics the ionic strength and pH of blood serum [25]. GST is diluted hydrochloric acid (HCl) and therefore expected to represent conditions of relevance for pitting or crevice corrosion of stainless steel, ALF is a highly complexing solution shown to form complexes with released Cr, Ni, and Fe [26], and PBS represents relatively benign exposure conditions. All three fluids kept their initial pH throughout the 24 h exposure period. The chemical composition and pH of each fluid is summarized in Table 1. All chemicals were of analytical grade and weighed by means of an analytical balance (Sartorius ED124S) into volumetric flasks, followed by mixing with ultrapure water (resistivity-18.2 MΩcm, Millipore, Sigma), used as solvent. All fluids were prepared on the same day as the exposure. The pH was adjusted to stipulated levels using 0.1 M NaOH or 65% HNO_3, and checked using a pH meter (Orion Star).

After the immersion period, the coupons were rinsed with ultrapure water (thereafter wasted), and dried with nitrogen gas at room temperature, before stored in a desiccator (<10% relative humidity) prior to the surface analysis. All sample solutions (after exposure) were acidified to pH < 2 using 45 μL ultrapure 65% HNO_3 prior to trace metal analysis (standard procedure for metal analysis).

All vessels and containers used in the exposures and for sample storage were acid cleaned with 10% HNO_3 for at least 24 h before rinsed four times with ultrapure water and dried in ambient laboratory conditions.

2.2. Surface chemical characterization

Surface chemical analysis was performed by a combination of ToF-SIMS and XPS on unexposed and exposed 316L surfaces.

ToF-SIMS (TOF-SIMS IV, ION-TOF GmbH, Germany) was employed for depth profiling of the surface oxide. The coupon surface was bombarded with a pulsed (~1 ns) 25 keV Bi_3^+ primary ion beam (target current ~ 1 pA), which generates ions from the outermost 1–3 nm of the surface. These secondary ions were extracted by an electric field and their times of flight through a reflector tube were determined and converted to mass to charge (m/z) ratios via known species such as hydrogen, carbon, hydrocarbons and other known species when necessary, constructing a spectrum of secondary ion mass. A low energy electron beam flooded over the sample to compensate build-up of charge caused by the bombardment of the positive primary ion beam. The base pressure of the main chamber of the instrument was about 10^{-7} mbar. Secondary ion mass spectra were collected from 128 × 128 pixels over the rastered area with two shots of pulsed primary ion beam per pixel. Negative ion mass spectra were calibrated using H^-, C^- and Fe^- signals. Images of given ions were acquired by mapping the ion intensity against the pixels with a resolution in the order of a couple of micrometers. Depth profiles were generated by alternatively sputtering the surface for 1 s with a 3 keV Cs^+ beam over an area sized 200 μm × 200 μm and analyzing an area of 128 μm × 128 μm within the sputtered area using a 25 keV Bi_3^+ primary ion beam. The sputter rate was estimated to ~ 0.15 nm/s. Data acquisition and processing were performed using ION-TOF's SurfaceLab 7 software. Duplicate coupons were investigated for each solution, and two depth profiles were acquired for each coupon.

XPS analysis was carried out with a Kratos AXIS Supra X-ray photoelectron spectrometer using a monochromatic Al Kα source (15 mA, 15 kV). All elements except hydrogen and helium can be detected within the outermost surface (7–10 nm) with detection limits ranging from 0.1−0.5 at.-% depending on the element. The instrument work function was calibrated to give a binding energy (BE) of 83.96 eV for the Au $4f_{7/2}$ line for metallic gold and the spectrometer dispersion was adjusted to give a BE of 932.62 eV for the Cu $2p_{3/2}$ line of metallic Cu. The Kratos charge neutralizer system was used on all coupons. Survey scan analyses were carried out on areas sized 300 × 700 μm using a pass energy of 160 eV, and high resolution analysis used a pass energy of 20 eV. Spectra were charge-corrected to the main line of the C 1 s spectrum (adventitious carbon) set to 284.8 eV. Two different surface areas on one coupon were investigated for each solution and the spectra were analyzed using the CasaXPS software (version 2.3.14) [27]. Estimates of oxide thicknesses were made as described by Strohmeier [28], Carlson and McGuire [29] and modified by Biesinger et al. [30]. If the metal to oxide ratio can be determined for a thin oxide (~0–9 nm) and if the inelastic mean free path (IMFP, λ) of the metal (λ_m) and oxide (λ_{ox}) (or a weighted combination of oxides) is known (or can be calculated), the oxide thickness can be calculated as in Eq. (1).

$$d = \lambda_{ox}\sin\theta \ln((N_m\lambda_m I_{ox})/(N_{ox}\lambda_{ox}I_m) + 1) \quad (1)$$

where θ is the photoelectron take-off angle (90° in this study), I_{ox} and I_m are percentages of the oxide and metal peaks from the high-resolution spectrum, and N_m and N_{ox} are volume densities of the metal atoms in the metal and oxide, respectively. More details are given in Tables S2 and S3 (supplementary information).

2.3. Trace metal analysis in solution

Inductively coupled plasma mass spectrometry (ICPMS, Agilent 7700x) was used to quantify released amounts of Cr, Mn, Fe, Co and Ni in solution after 24 h of exposure. Limits of detection (LOD) and limits of quantification (LOQ) are summarized in Table 2, based on 3 and 10 times the standard deviation of the noise level, respectively. The LODs and LOQs were adjusted to consider any dilution of the samples performed to reduce matrix effects induced by Na

Table 1
Components (g/L) and pH of the synthetic fluids: artificial gastric fluid (GST), artificial lysosomal fluid (ALF) and phosphate buffered saline (PBS).

Chemicals	GST, pH 1.5	ALF, pH 4.5	PBS, pH 7.4
$MgCl_2$	–	0.05	–
NaCl	–	3.21	8.77
Na_2HPO_4	–	0.071	1.28
Na_2SO_4	–	0.039	–
$CaCl{\cdot}2H_2O$	–	0.128	–
$C_6H_5Na_3O_7{\cdot}2H_2O$ (trisodium citrate)	–	0.077	–
KH_2PO_4	–	–	1.36
$C_6H_8O_7$ (citric acid)	–	20.8	–
H_2NCH_2COOH (glycine)	–	0.059	–
$C_4H_4O_6Na_2{\cdot}2H_2O$ (disodium tartrate)	–	0.090	–
$C_3H_5NaO_3$ (sodium lactate)	–	0.085	–
$C_3H_3O_3Na$ (sodium pyruvate)	–	0.086	–
NaOH	–	6.00	–
HCl 25%	4	–	–

Table 2
Limits of detection (LODs) and limits of quantification (LOQs) for the metals analyzed by means of ICPMS.

Element	LOD (μg/L)	LOQ (μg/L)
Cr	0.17	0.50
Mn	0.51	1.5
Fe	2.8	8.4
Co	0.37	1.1
Ni	0.79	2.4

and Cl ions in solution. Recoveries of spiked matrix samples were in the 70–130% range of the nominal values and recoveries of quality controls samples were analyzed during the measurements with < ±15% difference from nominal values.

Average sample concentrations of three independent samples are presented with the corresponding blank concentration (solution sample exposed without a 316L coupon) subtracted. Released amounts of metals expressed as μg/cm^2 correspond to the blank-corrected concentration of released metals (μg/L) multiplied with the solution volume (L) and divided by the exposed surface area (cm^2) of the coupon.

3. Results and discussion

3.1. ToF-SIMS compositional depth profiling

Fig. 1 displays depth profiles of selected negative ions of the stainless steel 316L, which include ions representing metal oxides (MeO_x^-), metallic species (Me_2^-) and solution components (PO_3^-, PO^-, Cl_2^-, Cl^-). These metal ions are conventionally used to characterize stainless steel surfaces [3,11]. As proposed in the literature [3], the depth profiles can be divided into three regions corresponding to the oxide, the modified alloy layer, and the metallic substrate, see Fig. 1. The oxide is defined as depth at which the integrated peak intensity of the Cr oxide (CrO_3^-/CrO_3H^-) has been reduced with 20% from its maximum. The intermediate region between the oxide and the metallic substrate is assigned as the modified alloy layer and defined as the region between the oxide and when the intensity plateau of metallic Fe (Fe_2^-) has reached 80% of its maximum. The sputtering time range was determined from where the intensities of ions in their depth profiles plateaued, which suggests the complete removal of the modified alloy layers and the exposure of the bulk of 316L.

All profiles showed a sharply increased signal in the first couple of seconds of sputtering, mainly due to the removal of the adventitious carbon [31] present at the outermost part of the surface. In the surface oxide region, most coupons revealed an oxide comprised of Fe and Cr oxides as the most predominant components and to a lesser extent Mo oxide (Fig. 1). The FeO_2^- and MoO_2^- profiles showed very similar in-depth distributions which were concentrated within the outermost oxide, whereas CrO_3H^- in most cases appeared slightly further away from the surface. This indicates a bi-layered oxide structure with a predominance of Fe and Mo oxides located in the outer layer and of Cr oxides enriched in the inner layer. These findings agree with reports on air-formed and water-immersed surface oxides on stainless steel 316L and similar grades [3,11,32,33]. It has been suggested that, due to the abundance of Fe metal, Fe oxides are initially formed followed by Cr oxides [34]. However, for the coupons exposed to GST (Fig. 1b), the Cr, Mo and Fe oxide peaks appeared at approximately the same position (after sputtering ≈ 4 s). The enrichment of Cr within the outermost surface oxide under acidic conditions is in accordance with previous findings [5,15]. The oxidized Fe, Cr, and Mo ion profiles slowly decreased in intensity through the film and reached a plateau adjacent to the metallic substrate.

The oxidized Co ion is not included in Fig. 1, since its intensity, indicative of oxidized Co fragments (e.g., Co^-, CoO^-, CoO_2^-), was extremely low compared to the FeO_2^-, CrO_3^-/CrO_3H^- and MoO_2^- ions. There was also an overlap between oxidized Co and other species, most importantly Ni since the mass to charge ratio of Co^- (58.9332) interferes with NiH^- (58.9432). This interference is clearly illustrated in Fig. S1 (supplementary material) and precludes any definitive conclusions in measuring Co^- and any Co oxide ions.

Coupons exposed to ALF and PBS (Fig. 1c and 1d) showed depth profiles containing phosphate fragments, with a higher concentration for coupons after exposure to PBS. PO^- was used for the coupons exposed to PBS due to very strong PO_3^- peak intensities that saturated the detector, see Figure S2 (supplementary material). The profiles of PO^- and PO_3^- appeared to strongly correlate with the metal oxide signals, indicating their incorporation within the oxide as a result of exposure to ALF and PBS. Cl^- was detected on all coupons, with stronger signals for exposed compared with unexposed coupons, especially in GST. Since the Cl^- signal saturated the detector, Cl_2^- was used instead, Fig. 1b.

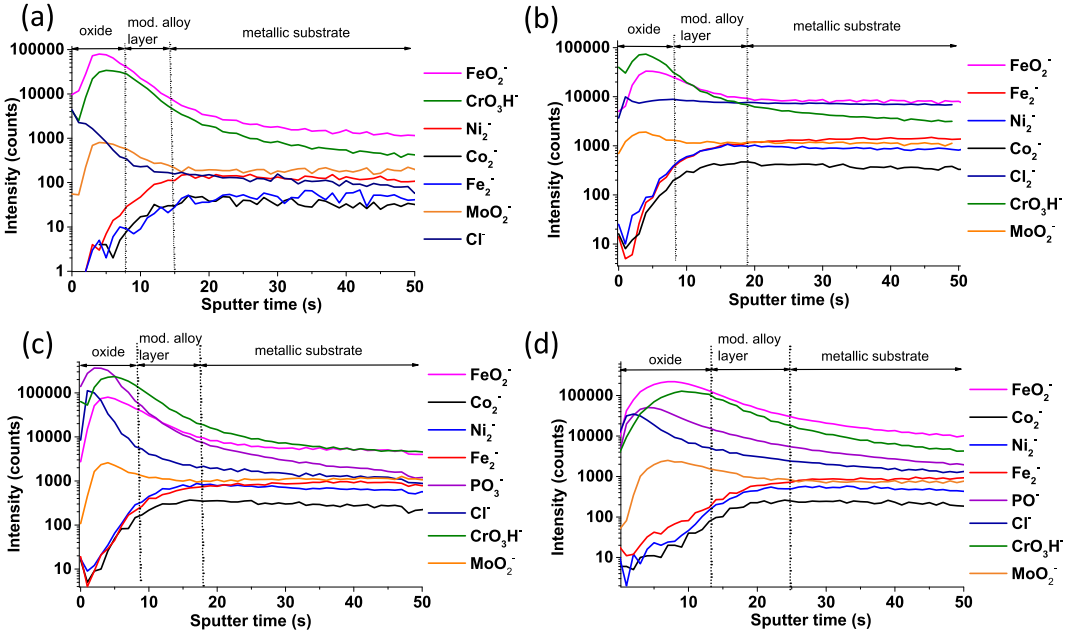

Fig. 1. Representative ToF-SIMS depth profiles for 316L: unexposed (a), exposed to GST (b), to ALF (c) and to PBS (d) for 24 h at 37 °C. The depth profiles provide average information from an area sized 128 μm × 128 μm. Cl_2^- in (b) and PO^- in (d) are presented, instead of Cl^- and PO_3^-, for the coupons exposed to GST and PBS, respectively, due to the strong signals of Cl^- and PO_3^-, which saturate the detector. A sputter time of 1 s represents the removal of ≈0.15 nm (a sputter time of 50 s corresponds to a depth of 7.5 nm). Presented intensities are integrated from the ToF-SIMS mass spectra, and the results are plotted using a logarithmic scale.

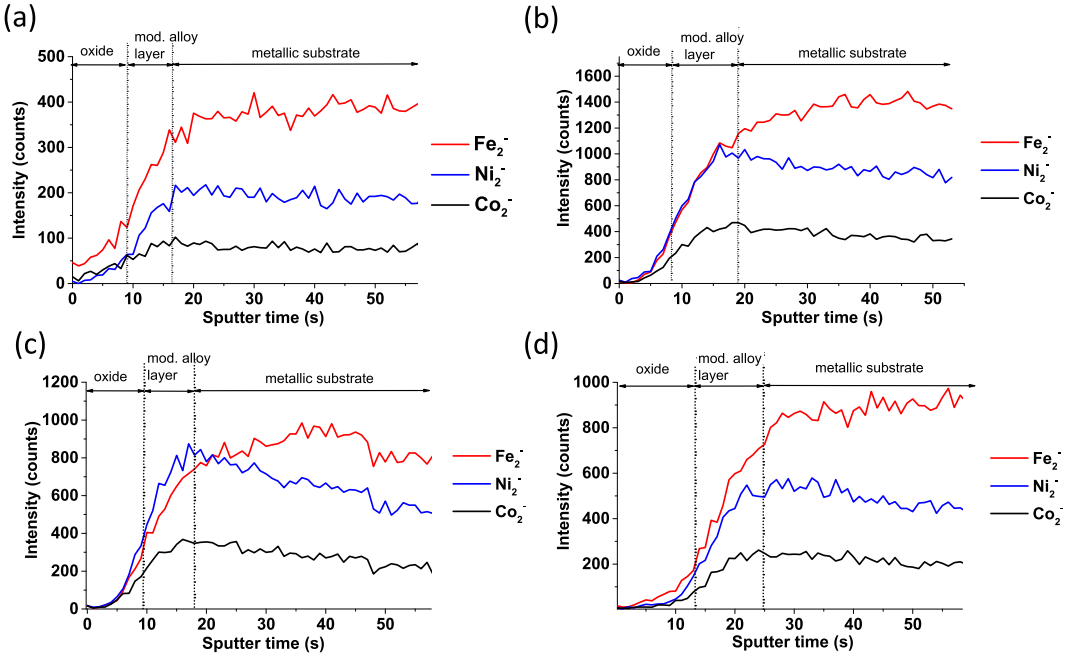

Fig. 2. Magnified ToF-SIMS depth profiles of 316L from Fig. 1, focusing on ions corresponding to metallic species: unexposed (a), exposed to GST (b), to ALF (c) and to PBS (d) for 24 h at 37 °C. Note that the intensity is plotted in a linear scale versus sputtering time.

No metallic Cr profile was observed due to its very low intensity as a result of low secondary emission yield [35]. The modified alloy layer (Fig. 1), which is the transition region between the oxide and the metal substrate, was characterized by progressively increased signals of metallic compounds (Fe_2^-, Ni_2^- and Co_2^-) and concomitantly reduced signals of metal oxides, e.g., MeO_x^- (with Me = Cr, Fe, Mo). Fig. 2 shows the depth profiles of metallic Fe, Ni and Co versus sputtering time in a linear scale. The Fe_2^- signal gradually increased to a plateau further into the substrate, whereas the Ni_2^- signal tended to be highest adjacent to the interface between the modified alloy layer and the substrate. The metallic Co (Co_2^-) signal, though relatively weak, followed the trend of the Ni_2^- signal. These results suggest that this region is mainly composed of metallic Fe and enriched with Ni and Co at the metal/oxide interface.

2D chemical images (128 μm × 128 μm) of the differently exposed coupons are shown in Figs. S3-S6 (supplementary material), based on ToF-SIMS measurements for selected ions representing metallic, metal oxide and phosphate species of the surface. The signals from the metallic fragments (Cr_2^-, Fe_2^-, Ni_2^-, Co_2^-) were evenly distributed across the surface. The Fe and Cr oxide signals showed some variation across the surface for coupons exposed in both ALF and PBS, while this was not the case for the Mo oxide. The phosphate signals correlated with stronger oxide signals for the coupons exposed in ALF and PBS. Most importantly, no heterogeneous distribution of the Co signal could be discerned.

The presence of oxidized Co in the surface oxide could not be completely resolved by means of ToF-SIMS due to its low concentration and interference with other species. The generation of secondary ions from a surface during ToF-SIMS analysis can be affected by many factors, including the presence of surface heterogeneities and differences in chemical stability of various surface species [36]. Surface-sensitive quantitative XPS analysis was therefore employed to acquire quantitative compositional and complementary information.

3.2. Quantitative surface compositional analysis by means of XPS

Fig. 3 presents the relative atomic percent (at.-%) of surface species on the unexposed and exposed coupons investigated by means of XPS. Their relative fractions are based on curve fitting of high resolution XPS spectra of Fe 2p, Ni 2p, Co 2p and Cr 2p [30,37]. Similar to the ToF-SIMS results, the surface oxides were in all cases mainly composed of oxidized Fe (15–51 at.-%) and Cr (16–50 at.-%) and to a minor extent Mo (1–2 at.-%). Exposures to synthetic body fluids resulted in a surface oxide composed of less amounts of oxidized Fe (from 51 to 15–33 at.-%), most evident for exposures in GST and ALF. Simultaneously, the relative content of oxidized Cr (especially $Cr(OH)_3$ species) increased from 16 at.-% within the native oxide to 40–50 at.-% upon immersion in GST and ALF. This can be explained by the preferential dissolution of Fe compared to Cr during immersion under acidic conditions [35,38,39]. The Cr oxides were identified in their trivalent form (Cr_2O_3 and/or $Cr(OH)_3$), providing good corrosion resistance [15]. Interestingly, small amounts of Co(III) were observed after exposure to PBS. No

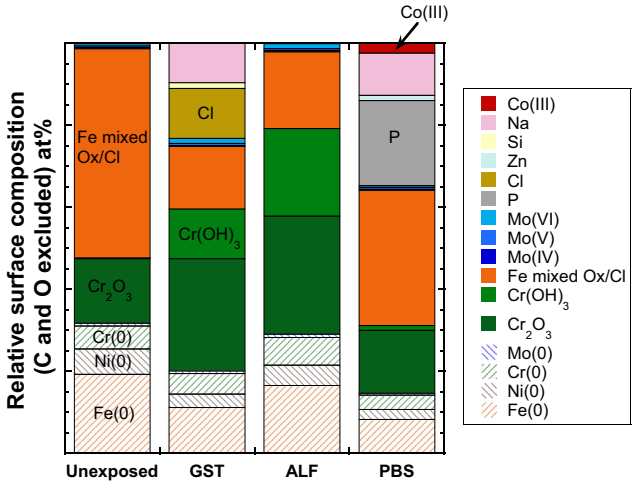

Fig. 3. Relative atomic percentage (at.-%) of detected species (C and O excluded) in the outermost surface oxide of 316L identified by means of XPS, prior to (unexposed) and after 24 h exposure to GST (pH 1.5), ALF (pH 4.5) and PBS (pH 7.4). The results reflect average values of two different surface areas on each coupon. Raw data is given in Table S1 (supplementary material).

Ni oxide was noted in the outermost surface of any of the investigated coupons. Metallic Ni signals were identified for all coupons, related to the enrichment of Ni beneath the surface oxide as observed by means of ToF-SIMS (Figs. 1 and 2) and in agreement with previous findings [3,11,40]. Solution constituents were observed on the surface including Cl (as Cl^-) in GST and P (as PO_4^{2-}) in PBS. The presence of phosphate on the coupons exposed to PBS may indicate the precipitation of Co(III)-phosphate from solution [41,42]. It should be noted that the phosphate concentration in PBS was about 10 times higher than in human blood [43], which means that this study cannot answer the question whether a similar precipitation of Co(III)-phosphate would be expected in-vivo. Sodium (Na), silicon (Si) and zinc (Zn), either from the solutions or the surrounding environment, were also observed on the surfaces.

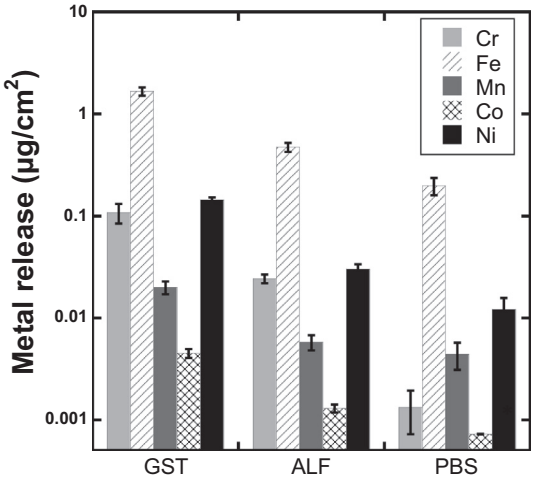

Fig. 4. Amount of released metals (µg/cm^2) from 316L exposed for 24 h to GST, ALF, and PBS at 37 °C. In PBS, the Co concentration exceeded the LOD but not the LOQ. The error bars represent the standard deviation of independent triplicate samples.

3.3. Metal release determined by means of ICPMS

Fig. 4 shows the amount of released Cr, Fe, Mn, Co, and Ni per surface area (µg/cm^2) for 316L after 24 h of exposure to GST (pH 1.5), ALF (pH 4.5) and PBS (pH 7.4) at 37 °C. Consistent with previous findings [2], the released amount of each element was highly pH and solution-dependent, with the highest release in GST, followed by ALF and PBS. In the case of ALF, the release was, as previously demonstrated, not primarily caused by the solution pH but rather by ligand-induced processes connected to complexation with citric acid [26,44]. Fe was predominantly released (86–91 wt-% of total Fe + Cr + Ni + Mn + Co release), followed by Ni (5.6–7.4 wt-% of total release), Cr (0.6–5.6 wt-% of total release), Mn (1.0–2.0 wt-% of total release), and Co (0.23–0.34 wt-% of total release), see Table S2. The results show that Fe (≈ 70 wt-% in the bulk) was preferentially released into all solutions, Mn and Co were approximately released in proportion to their bulk compositions (0.9 wt-% Mn and 0.2 wt-% Co), whereas Cr and Ni were released to a lower extent than their bulk compositions (17 wt-% Cr and 10 wt-% Ni).

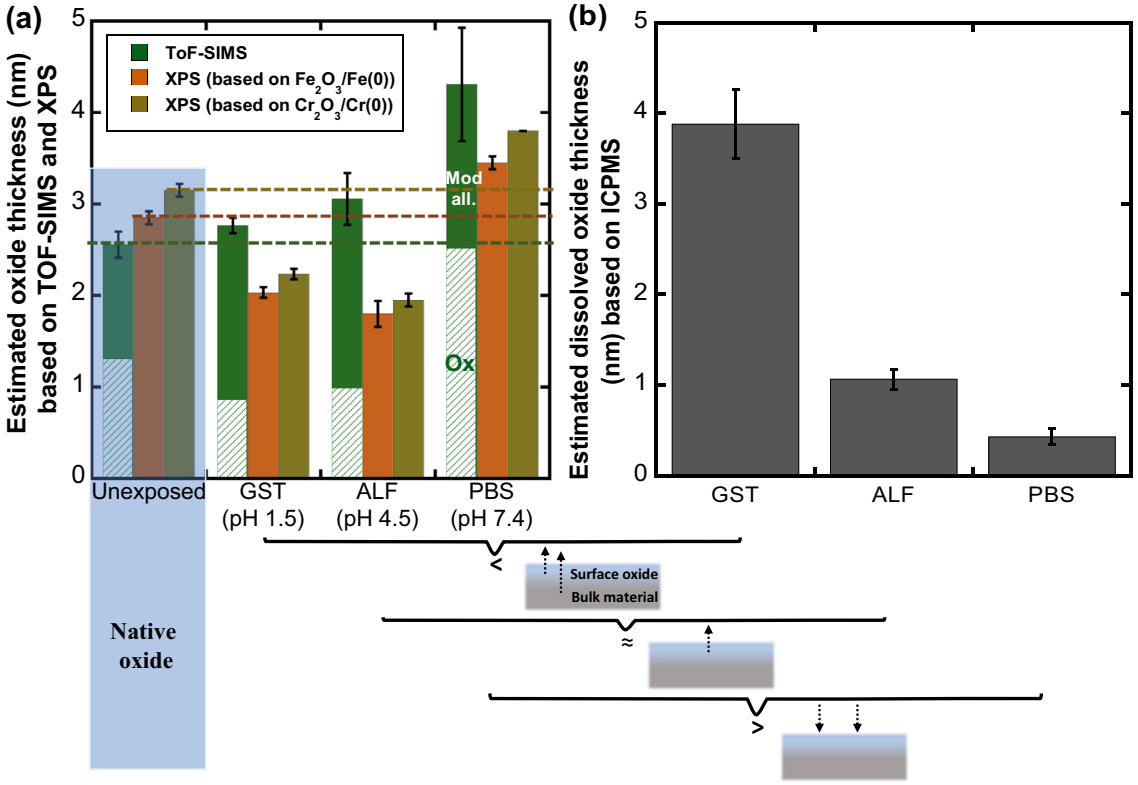

Fig. 5. Changes in oxide thicknesses before and after exposure based on ToF-SIMS and XPS results (a), and dissolved oxide thickness calculated from ICPMS release data (b). The ToF-SIMS results include both the surface oxide (Ox) and the modified alloy (Mod. all.) layer thicknesses (details in Fig. S7 and Table S3). The error bars represent the standard deviation of quadruplicate ToF-SIMS depth profiles (two profiles each from two independent coupons), duplicate/triplicate areas of XPS (see Tables S4-S5) and triplicate (independent) samples of the ICPMS results (see Table S6). The reduction in oxide thickness based on ToF-SIMS and XPS was smaller than (<), or equal to (≈), the dissolved oxide thickness estimated from the released amounts of metals. The increase in oxide thickness and measured oxide thickness based on ToF-SIMS and XPS was larger (>) than the estimated dissolved oxide thickness. Schematic illustrations of proposed interfacial processes are included.

3.4. Oxide thickness estimations

The analytical results from ToF-SIMS and XPS were used to estimate changes in oxide thickness before and after reformation in the different synthetic fluids, and metal release data generated by ICPMS was used to calculate the average estimated thickness of the dissolved oxide, Fig. 5. All calculations assumed uniform changes in oxide thickness. Total amounts of released metals (total amount of Fe, Cr, Ni, Mn, Co, in $\mu g/cm^2$) were used to estimate the corresponding released/dissolved (hydr)oxide thickness, assuming an average (hydr)oxide density of 5 g/cm^3 [45] described in Eq. (2).

$$d(nm) = (\sum \frac{\mu g}{cm^2})/(5\frac{g}{cm^3}) \times 10 \quad (2)$$

Based on the ToF-SIMS and XPS results (Fig. 5a), it was concluded that the exposure in PBS resulted in an approximately 1 nm thicker surface oxide compared to the native oxide (from 2.6 to 3.2 nm to 3.5–4.3 nm). However, a lower extent of metals, corresponding to an approximate oxide thickness of 0.5 nm, was released into solution (Fig. 5b). These results indicate that oxide formation was favored over oxide dissolution in PBS. This is not surprising, as Fe and Cr oxides have very low solubility at a pH of 7.4, and any aqueous Fe and Cr ions would be expected to precipitate from solution to form Fe and Cr hydroxides or oxides [46,47].

According to XPS, exposure to ALF resulted in a reduced oxide thickness (from 2.6 to 3.2 nm to 1.8–2.0 nm), whereas the ToF-SIMS data rather indicated a slightly increased thickness (to 3.1 nm), Fig. 5a. The extent of measured metal release in ALF corresponded to a reduction in oxide thickness of approximately 1 nm (Fig. 5b), i.e. in line with the XPS findings. The corresponding mass of this thickness reduction was identical to the released mass determined in solution. This suggests that the released metals in ALF predominantly originated from the surface oxide rather than from the bulk alloy matrix. This is consistent with previous findings with surface complexation reactions as the predominant metal release mechanisms in citric acid solutions [26,48]. The relative content of oxidized metals within the surface oxide seemed to decrease (based on oxide to metal ratios determined with XPS and compositional findings in the outer oxide layer determined with ToF-SIMS), while the total surface layer (surface oxide and modified alloy layer) seemed to slightly increase in thickness. Similar to findings in ALF, exposure to GST resulted, according to the XPS results, in a reduced (approximately 1 nm) surface oxide thickness. ToF-SIMS measurements indicated a similar total surface oxide thickness (2.8 nm, including the modified alloy layer) as the thickness of the native surface oxide (2.6 nm) (Fig. 5a). Exposure to GST resulted in the highest extent of released metals, corresponding to an estimated dissolved surface oxide thickness of approximately 4 nm (Fig. 5b), which 4-fold exceeded the XPS-determined reduced surface oxide thickness. This implies that the released metals in GST originated not only from the surface oxide but also from the bulk material. The results in this acidic chloride-containing fluid indicate the presence and importance of surface defects [5].

3.5. Proposed Co release mechanism in the synthetic biological fluids

The most important mechanistic insights from this study are schematically summarized in Fig. 6. Co is proposed to be enriched, along with Ni, as a metallic impurity in the modified alloy layer beneath the surface oxide of stainless steel 316L. Co release into

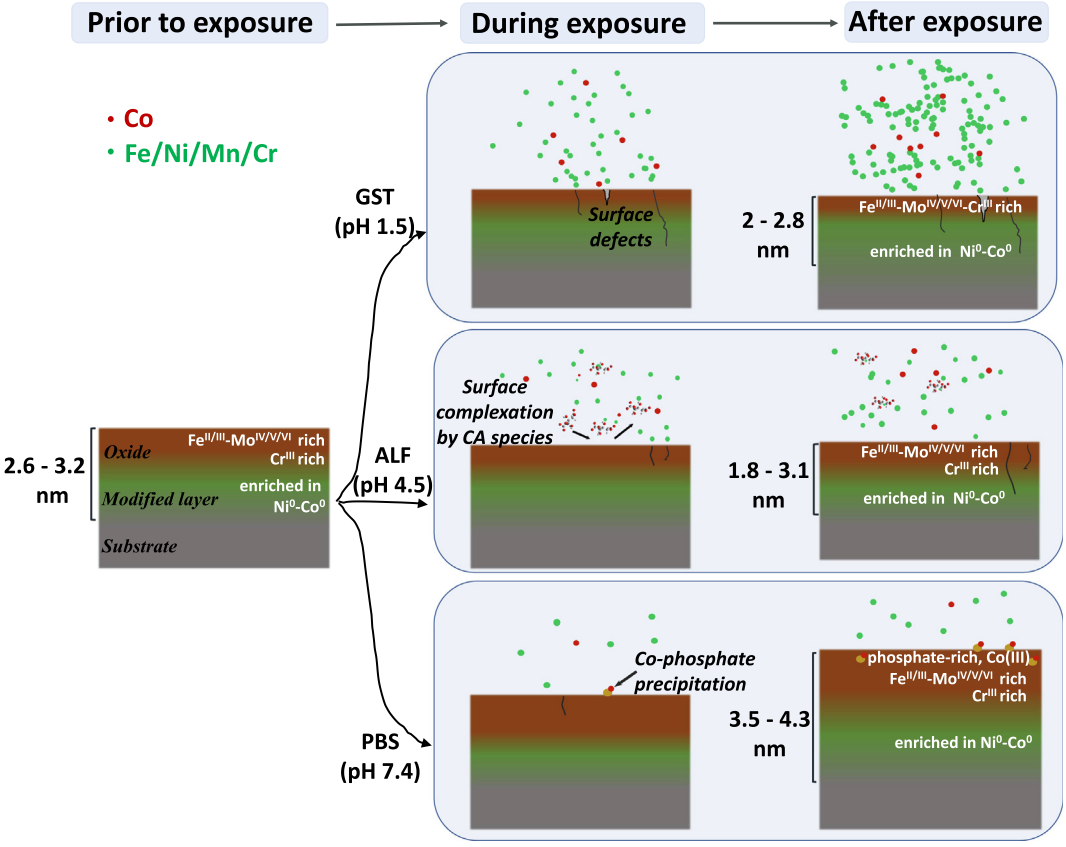

Fig. 6. Schematic overview of changes in surface composition and estimated surface oxide thickness of 316L and relative extent of released metals after 24 h of exposure at 37 °C to GST (pH 1.5), ALF (pH 4.5) and PBS (pH 7.4). CA – citric acid.

solution was a consequence of surface defects and surface oxide reformation upon exposure in the different synthetic fluids.

Previous studies on 316L exposed to the investigated synthetic body fluids show strongly reduced metal release rates (including Co) with time, and considerably lower extent of metal release after an initial passivation process (either in nitric acid, in the investigated synthetic body fluids, or other acids) [5,48,49].

During this initial passivation process, the oxide partially dissolves, and surface defects passivate. However, most surface defects, including formed pits, remain or occur upon exposure to GST [5], which facilitates the release of Co and other alloying elements into solution both from the surface oxide and from the bulk matrix. In ALF, surface complexation by citric acid species has previously been shown to be the dominating metal release mechanism [26,46].

In the case of PBS, in which oxide formation was favored over dissolution, released Co ions precipitated onto the surface, possibly as Co-phosphates [41,42]. As the XPS results (Section 3.2) identified Co as Co(III), this may suggest precipitation of Co(III) phosphate. Since the very strong phosphate signals of the ToF-SIMS spectra correlated with the metal oxide signals after exposure to PBS, the Co-phosphates are proposed to be incorporated in the outermost surface layer. This raises the question whether Co could be released upon subsequent exposure in more corrosive media. This requires further investigations. A recent study reported high amounts of Co released from the surface of a stainless steel container in PBS, being pre-exposed to PBS and Co ions released from cobalt alloys [42].

From a regulatory perspective, it makes sense to suggest that Co is not, or only during the initial passivation period, released from stainless steel 316L under conditions for which the passive surface oxide is stable, such as in PBS and ALF (after the passivation process). However, under conditions where localized corrosion could occur, such as in crevices and in hydrochloric acid, small amounts of Co can be released along with Ni from the enriched metallic layer present beneath the surface oxide.

4. Conclusions

The aim of this study was to gain mechanistic insight in the release process of Co from stainless steel 316L by determining the location of Co impurities in the outermost surface upon exposure to three synthetic biological fluids. The following main conclusions were drawn:

- ToF-SIMS and XPS analysis revealed that the surface oxide of 316L has a duplex structure with $Fe^{II}/^{III}$-$Mo^{IV}/^{V}/^{VI}$ enriched in the outer oxide and Cr^{III} enriched in the inner oxide, both before and after exposure to ALF (pH 4.5) and PBS (pH 7.4). Exposures to GST (pH 1.5) resulted in an outermost oxide predominantly composed of $Fe^{II}/^{III}$-$Mo^{IV}/^{V}/^{VI}$-Cr^{III} species. Exposures in all fluids showed a homogenous distribution of metallic Co and its co-location with metallic Ni beneath the surface oxide.
- Trace amounts of Co were released along with other metals in all fluids. The highest amounts of released Fe, Cr, Ni, Mn, and Co were observed in GST (pH 1.5), followed by ALF (pH 4.5) and PBS (pH 7.4). Fe was preferentially released, whereas Cr and Ni were released to a lower extent than their respective proportions in the bulk. Co and Mn were released in proportion to their respective bulk composition.
- When comparing changes in estimated surface oxide thicknesses before and after exposure based on results generated by means of XPS and ToF-SIMS to the corresponding dissolved surface oxide thickness estimated from ICPMS findings, it was evident that oxide formation exceeded oxide dissolution in PBS. The reduction in oxide thickness was equal to the oxide dissolution determined from the amount of released metals in ALF. In GST, the oxide dissolution estimated from the amount of released metals was four-fold higher than the estimated reduced oxide thickness based on XPS and ToF-SIMS findings, which implies a role of surface defects.
- XPS detected oxidized Co(III) within the surface oxide after exposure to PBS, and ToF-SIMS showed laterally and spatially overlapping phosphate and metal oxide signals. These findings may suggest the precipitation and incorporation of Co-phosphate in the surface oxide.

Funding

This work was supported by the Swedish Steel Producer's Association (Jernkontoret) [Axel Ax:sons forskningsfond 2020], Chinese Scholarship Council, Beijing, China [grant number: 201700260221]; Wolfe-Western fellowship, Canada [grant number: 2020]; Canada Research Chairs Program [grant number: 950 – 233099].

Data availability

The raw data required to reproduce the above findings are available to download from https://osf.io/a8wkv/. The processed data required to reproduce the above findings are available to download from https://osf.io/a8wkv/.

CRediT authorship contribution statement

Xuying Wang: Conceptualization, Methodology, Formal analysis, Writing – original draft, Writing – review & editing, Visualization. **Jonas Hedberg:** Methodology, Formal analysis, Investigation, Writing – review & editing, Visualization. **Heng-Yong Nie:** Methodology, Investigation, Writing – review & editing. **Mark C. Biesinger:** Methodology, Investigation, Writing – review & editing. **Inger Odnevall:** Conceptualization, Writing – review & editing, Supervision, Project administration, Funding acquisition. **Yolanda S. Hedberg:** Conceptualization, Methodology, Writing – review & editing, Visualization, Supervision, Project administration, Funding acquisition.

Declaration of Competing Interest

The authors declare that they have no known competing financial interests or personal relationships that could have appeared to influence the work reported in this paper.

Appendix A. Supplementary material

Supplementary data to this article can be found online at https://doi.org/10.1016/j.matdes.2022.110524.

References

[1] B. Lynch, S. Neupane, F. Wiame, A. Seyeux, V. Maurice, P. Marcus, An XPS and ToF-SIMS study of the passive film formed on a model FeCrNiMo stainless steel surface in aqueous media after thermal pre-oxidation at ultra-low oxygen pressure, Appl. Surf. Sci. 554 (2021) 149435.
[2] Y.S. Hedberg, I. Odnevall Wallinder, Metal release from stainless steel in biological environments: A review, Biointerphases 11 (1) (2016) 018901, https://doi.org/10.1116/1.4934628.
[3] L. Wang, A. Seyeux, P. Marcus, Thermal stability of the passive film formed on 316L stainless steel surface studied by ToF-SIMS, Corros. Sci. 165 (2020) 108395.
[4] N. Shetty, V. Olsovcova, R. Versaci, Sensitivity of ambient dose equivalent to the concentration of cobalt impurity present in stainless steel, J. Phys. Conf. Ser. 1046 (2018) 012005.

[5] X. Wang, J.J. Noël, I. Odnevall Wallinder, Y.S. Hedberg, Metal bioaccessibility in synthetic body fluids–A way to consider positive and negative alloying effects in hazard assessments, Mater. Des. 198 (2021) 109393.
[6] EC, Regulation (EC) No 1907/2006 of the European Parliament and of the Council of 18 December 2006 concerning the Registration, Evaluation, Authorisation and Restriction of Chemicals (REACH), establishing a European Chemicals Agency, amending Directive 1999/45/EC and repealing Council Regulation (EEC) No 793/93 and Commission Regulation (EC) No 1488/94 as well as Council Directive 76/769/EEC and Commission Directives 91/155/EEC, 93/67/EEC, 93/105/EC and 2000/21/EC. https://eur-lex.europa.eu/legal-content/EN/TXT/?uri=CELEX%3A02006R1907-20140410, 2006, (accessed 22 October 2021).
[7] N. Lombaert, C. Mackie, V. Verougstraete, T. Brouwers, F. Van Assche, A. Oller, Use of bioelution as a screening tool for characterisation of substances, Am. J. Analyt. Chem. 9 (2018) 134.
[8] ECHA, Harmonised classification - Annex VI of Regulation (EC) No 1272/2008 (CLP Regulation). https://echa.europa.eu/information-on-chemicals/cl-inventory-database/-/discli/details/34808, 2008 (accessed 22 October 2021).
[9] M. Resources, Comments and response to comments on CLH: proposal and justification. https://echa.europa.eu/documents/10162/39a20032-2e9b-d383-7050-e052d38a5e14, 2017 (accessed 22 October 2021).
[10] K.E. Heim, R. Danzeisen, V. Verougstraete, F. Gaidou, T. Brouwers, A.R. Oller, Bioaccessibility of nickel and cobalt in synthetic gastric and lung fluids and its potential use in alloy classification, Regul. Toxicol. Pharmacol. 110 (2020) 104549.
[11] Z. Wang, F. Di-Franco, A. Seyeux, S. Zanna, V. Maurice, P. Marcus, Passivation-induced physicochemical alterations of the native surface oxide film on 316L austenitic stainless steel, J. Electrochem. Soc. 166 (11) (2019) C3376–C3388.
[12] Z. Wang, A. Seyeux, S. Zanna, V. Maurice, P. Marcus, Chloride-induced alterations of the passive film on 316L stainless steel and blocking effect of pre-passivation, Electrochim. Acta. 329 (2020) 135159.
[13] Z. Wang, Z. Feng, L. Zhang, Effect of high temperature on the corrosion behavior and passive film composition of 316 L stainless steel in high H2S-containing environments, Corros. Sci. 174 (2020) 108844.
[14] B. Lynch, Z. Wang, L. Ma, E.M. Paschalidou, F. Wiame, V. Maurice, P. Marcus, Passivation-induced Cr and Mo enrichments of 316L stainless steel surfaces and effects of controlled pre-oxidation, J. Electrochem. Soc. 167 (2020).
[15] C.-O.-A. Olsson, D. Landolt, Passive films on stainless steels—chemistry, structure and growth, Electrochim. Acta. 48 (9) (2003) 1093–1104.
[16] I. Olefjord, B.-O. Elfstrom, The composition of the surface during passivation of stainless steels, Corrosion 38 (1) (1982) 46–52.
[17] S.-X. Li, Y.-N. He, S.-R. Yu, P.-Y. Zhang, Evaluation of the effect of grain size on chromium carbide precipitation and intergranular corrosion of 316L stainless steel, Corros. Sci. 66 (2013) 211–216.
[18] M. Matula, L. Hyspecka, M. Svoboda, V. Vodarek, C. Dagbert, J. Galland, Z. Stonawska, L. Tuma, Intergranular corrosion of AISI 316L steel, Mater. Charact. 46 (2-3) (2001) 203–210.
[19] M.A. Baker, J.E. Castle, The initiation of pitting corrosion at MnS inclusions, Corros. Sci. 34 (4) (1993) 667–682.
[20] P. Schmuki, H. Hildebrand, A. Friedrich, S. Virtanen, The composition of the boundary region of MnS inclusions in stainless steel and its relevance in triggering pitting corrosion, Corros. Sci. 47 (5) (2005) 1239–1250.
[21] EU, Nickel Directive: European Parliament and Council Directive 94/27/EC of 30 June 1994: Amending for the 12th time Directive 76/769/EEC on the approximation of the laws, regulations and administrative provisions of the Member States relating to restrictions on the marketing and use of certain dangerous substances and preparations. https://eur-lex.europa.eu/LexUriServ/LexUriServ.do?uri=OJ:L:1994:188:0001:0002:EN:PDF, 1994 (accessed 22 October 2021).
[22] CEN, Reference test method for release of nickel from all post assemblies which are inserted into pierced parts of the human body and articles intended to come into direct and prolonged contact with the skin, EN 1811:2011 +A1:2015, 2015.
[23] S.C. Hamel, B. Buckley, P.J. Lioy, Bioaccessibility of metals in soils for different liquid to solid ratios in synthetic gastric fluid, Environ. Sci. Technol. 32 (3) (1998) 358–362.
[24] W. Stopford, J. Turner, D. Cappellini, T. Brock, Bioaccessibility testing of cobalt compounds, J. Environ. Monitor. 5 (4) (2003) 675, https://doi.org/10.1039/b302257a.
[25] K. Midander, J. Pan, C. Leygraf, Elaboration of a test method for the study of metal release from stainless steel particles in artificial biological media, Corros. Sci. 48 (9) (2006) 2855–2866.
[26] Y. Hedberg, J. Hedberg, Y. Liu, I. Odnevall Wallinder, Complexation-and ligand-induced metal release from 316L particles: importance of particle size and crystallographic structure, BioMetals 24 (2011) 1099–1114.
[27] N. Fairley, V. Fernandez, M. Richard-Plouet, C. Guillot-Deudon, J. Walton, E. Smith, D. Flahaut, M. Greiner, M. Biesinger, S. Tougaard, Systematic and collaborative approach to problem solving using X-ray photoelectron spectroscopy, Appl. Surface Sci. Adv. 5 (2021) 100112.
[28] B.R. Strohmeier, An ESCA method for determining the oxide thickness on aluminum alloys, Surf. Interface. Anal. 15 (1) (1990) 51–56.
[29] T.A. Carlson, G.E. McGuire, Study of the x-ray photoelectron spectrum of tungsten—tungsten oxide as a function of thickness of the surface oxide layer, J. Electron. Spectrosc. 1 (2) (1972) 161–168.
[30] M.C. Biesinger, B.P. Payne, L.W.M. Lau, A. Gerson, R.S.C. Smart, X-ray photoelectron spectroscopic chemical state quantification of mixed nickel metal, oxide and hydroxide systems, Surf. Interface. Anal. 41 (4) (2009) 324–332.
[31] T.L. Barr, S. Seal, Nature of the use of adventitious carbon as a binding energy standard, J. Vac. Sci. Technol. 13 (3) (1995) 1239–1246.
[32] K. Shimizu, H. Habazaki, P. Skeldon, G.E. Thompson, G.C. Wood, GDOES depth profiling analysis of the air-formed oxide film on a sputter-deposited Type 304 stainless steel, Surf. Interface Anal. 29 (11) (2000) 743–746.
[33] S. Tardio, M.-L. Abel, R.H. Carr, J.E. Castle, J.F. Watts, Comparative study of the native oxide on 316L stainless steel by XPS and ToF-SIMS, J. Vac. Sci. Technol. 33 (5) (2015) 05E122, https://doi.org/10.1116/1.4927319.
[34] L. Ma, B. Lynch, F. Wiame, V. Maurice, P. Marcus, Nanoscale early oxidation mechanisms of model FeCrNi austenitic stainless steel surfaces at room temperature, Corros. Sci. 190 (2021) 109653.
[35] L. Wang, D. Mercier, S. Zanna, A. Seyeux, M. Laurent-Brocq, L. Perriere, I. Guillot, P. Marcus, Study of the surface oxides and corrosion behaviour of an equiatomic CoCrFeMnNi high entropy alloy by XPS and ToF-SIMS, Corros. Sci. 167 (2020) 108507.
[36] J. Grams, New Trends and Potentialities of ToF-SIMS in Surface Studies, New York, 2007.
[37] M.C. Biesinger, B.P. Payne, A.P. Grosvenor, L.W.M. Lau, A.R. Gerson, R.S.C. Smart, Resolving surface chemical states in XPS analysis of first row transition metals, oxides and hydroxides: Cr, Mn, Fe, Co and Ni, Appl. Surf. Sci. 257 (7) (2011) 2717–2730.
[38] V. Maurice, H. Peng, L.H. Klein, A. Seyeux, S. Zanna, P. Marcus, Effects of molybdenum on the composition and nanoscale morphology of passivated austenitic stainless steel surfaces, Faraday. Discuss. 180 (2015) 151–170.
[39] V. Maurice, W. Yang, P. Marcus, X-Ray photoelectron spectroscopy and scanning tunneling microscopy study of passive films formed on (100) Fe-18Cr-13Ni single-crystal surfaces, J. Electrochem. Soc. 145 (1998) 909.
[40] P. Marcus, Corrosion Mechanisms in Theory and Practice, third ed., United States, 2011.
[41] Y.S. Hedberg, I. Dobryden, H. Chaudhary, Z. Wei, P.M. Claesson, C. Lendel, Synergistic effects of metal-induced aggregation of human serum albumin, Colloids. Surf. B. Biointerfaces 173 (2019) 751–758.
[42] Z. Wei, V. Romanovski, L. Filho, C. Persson, Y.S. Hedberg, Metal release from a biomedical CoCrMo alloy in mixed protein solutions under static and sliding conditions: effects of protein aggregation and metal precipitation, J. Bio- Tribo-Corros. 8 (2022) 1–11.
[43] V.K. Bansal, Serum inorganic phosphorus, in: H.K. Walker, W.D. Hall, J.W. Hurst (Eds.), Clinical Methods: The History, Physical, and Laboratory Examinations, Butterworth Publishers, Boston, 1990, pp. 895-899.
[44] Y. Hedberg, N. Mazinanian, I. Odnevall Wallinder, Metal release from stainless steel powders and massive sheets–comparison and implication for risk assessment of alloys, Environ. Sci. Process. Impacts. 15 (2) (2013) 381–392.
[45] National Center for Biotechnology Information, PubChem Compound Summaries. https://pubchem.ncbi.nlm.nih.gov/, (accessed 22 October 2021).
[46] B. Beverskog, I. Puigdomenech, Pourbaix diagrams for the ternary system of iron-chromium-nickel, Corrosion 55 (11) (1999) 1077–1087.
[47] M. Pourbaix, Electrochemical corrosion of metallic biomaterials, Biomaterials 5 (3) (1984) 122–134.
[48] N. Mazinanian, Y.S. Hedberg, Metal release mechanisms for passive stainless steel in citric acid at weakly acidic pH, J. Electrochem. Soc. 163 (10) (2016) C686–C693.
[49] G.N. Flint, S. Packirisamy, Purity of food cooked in stainless steel utensils, Food Addit. Contam. 14 (2) (1997) 115–126.